COMPDYN 2015
5th ECCOMAS Thematic Conference on
Computational Methods in Structural Dynamics and Earthquake Engineering
M. Papadrakakis, V. Papadopoulos, V. Plevris (eds.)
Crete Island, Greece, 25–27 May 2015

METHODOLOGY FOR THE DEVELOPMENT OF STRUCTURE-SPECIFIC FRAGILITY CURVES FOR BRIDGES IN A ROADWAY NETWORK

Sotiria P. Stefanidou[1], **Andreas J. Kappos**[2]

[1] Department of Civil Engineering, Aristotle University of Thessaloniki
University Campus, Thessaloniki, 54124, Greece
e-mail: ssotiria@civil.auth.gr

[2] Department of Civil Engineering, City University London
Northampton Sq., London EC1V 0HB, UK
Andreas.Kappos.1@city.ac.uk

Keywords: Bridges; roadway networks; fragility curves; seismic capacity; uncertainty estimation; nonlinear analysis.

Abstract. *Recognising the key role of bridges within a roadway network and the substantial direct and indirect losses related to bridge damage, a new methodology for the development of bridge-specific fragility curves is proposed, intended for application to the bridges forming part of a roadway network. with a view to estimating seismic losses in the network. The key features of the proposed methodology are the explicit definition of critical limit states (damage thresholds) for bridge components, considering the effects of geometry, material strength, reinforcement, and loading properties on the component capacity; the methodology also includes the correlation of local to global damage and the estimation of uncertainty in both capacity and demand. Advanced analysis methods and tools (nonlinear static and response history analysis, IDA) are used for bridge component capacity and demand estimation, whereas Latin Hypercube Sampling is used for uncertainty treatment. Based on processing of a large volume of results from analyses of full bridges, a simplified methodology is developed for seismic demand assessment, involving the use of an elastic (generic) bridge model and response spectrum analysis; demand is then related to component capacity and bridge-specific fragility curves are readily derived. The methodology can be applied, using an ad-hoc developed software, to a large number of bridges(having different geometries and properties) within a network, and direct and indirect losses can then be assessed.*

1 INTRODUCTION

Damage due to recent earthquakes worldwide highlights the role of bridges as the most vulnerable component of a roadway system. In view of this, during the last two decades, several methodologies have been developed for the assessment of bridge vulnerability, mainly in the context of developing fragility curves.

Since fragility is the probability that bridge damage exceeds a specific threshold limit state value for a given level of earthquake intensity, the key issue in the methodologies proposed in the literature is the estimation of capacity and demand at the system [1] or component level [2]. Threshold limit state values for critical components are quantified in terms of local (curvature, rotation) [3], [4] or global parameters [5] based on experimental data [6]. The capacity spectrum (or capacity and demand spectra) method and nonlinear response history analysis are commonly proposed for the demand calculation, while in most cases analytical fragility functions are derived using the Probabilistic Seismic Demand Model (PSDA or IDA) [7], or response surface metamodels [8]. Finally, it should be noted that in most cases uncertainties in demand and capacity are considered in a 'lumped' way.

The main drawback of the existing methodologies is that they are either based on advanced analysis tools, increasing dramatically the computational cost when applied to a large bridge inventory, or on approximate methods that do not account for the seismic performance of all critical structural components, hence risking to miss potential failure modes in some cases.

In view of the above, the key objective of this paper is to put forward a new methodology for the derivation of bridge-specific fragility curves, feasible for application to a bridge inventory with a view to estimating seismic losses in the bridges, as well as in the roadway network [9]. In general, bridges in a roadway network have different geometries, structural systems and component properties, due to differences in the topography and the construction method selected (figure 1). Therefore, the proposed methodology aims to reconciliate two conflicting requirements, namely the need for a detailed and reliable estimation of bridge capacity and demand, and the broad and efficient applicability. To this purpose, the end product of the methodology involves an elastic (generic) 3d bridge model and elastic response spectrum analysis results for the derivation of fragility curves. However, different component (i.e. pier) types have been previously analysed in order to correlate local to global damage, assess the effect of different geometry, material, reinforcement and loading properties on component capacity, and finally derive empirical relationships for component threshold limit state values. Moreover, the seismic performance of bridges with different structural systems is investigated using advanced analysis methods (nonlinear response history analysis, IDA) and the results are incorporated in the simplified methodology proposed.

Figure 1: Different bridge types within a roadway network

2 BRIDGE CLASSIFICATION SCHEME

In the frame of a network loss assessment, the vulnerability of bridges having different geometries, structural systems and properties should be estimated. The most important step prior to fragility analysis is the definition of a classification scheme for the bridges in the network, based on the parameters deemed as the most significant with respect to the seismic response. Therefore, a slightly enhanced version of the classification system developed in the framework of the research programme ASProGE [1], was adopted for the bridges of the roadway network of Greece. A three-digit code is used for each bridge type; the first digit denotes the pier type, the second the deck type, and the third the type of pier-to-deck connection (Table 1).

Code X1 *Pier Description*	**Code X2** *Deck Description*	**Code X3** *Pier-Deck Connection*
1 : Single Column (Solid)	1 : Slab (Solid or with voids)	1 : Monolithic
2 : Single Column (Hollow)	2 : Box girder	2 : Bearings
3 : Multi-column	3 : Simply supported pre-cast- prestressed beams	3 : Combination of monolithic & bearing
4 : Wall-type		
5 : V-shaped		

Table 1: Classification scheme proposed for Greek bridges.

3 DESCRIPTION OF THE METHODOLOGY FOR THE DERIVATION OF BRIDGE SPECIFIC FRAGILITY CURVES

Seismic performance of bridges is highly dependent on the structural system and properties of different components, namely piers, abutments, and bearings. Therefore, the first stage of the proposed methodology is to define the capacity of components, based on the results of inelastic analysis, considering different failure modes. Component limit states (minor, moderate, major and collapse), are qualitatively described based on experimentally observed damage sequence and performance and quantified defining threshold limit state values in terms of global engineering demand parameter (displacement), dependent on component geometry, reinforcement, material and loading properties. Uncertainty in capacity, namely in the damage threshold definition, is estimated using reduced Monte Carlo (Latin Hypercube Sampling) simulation for each component. The second stage is the development of a simplified 3d model

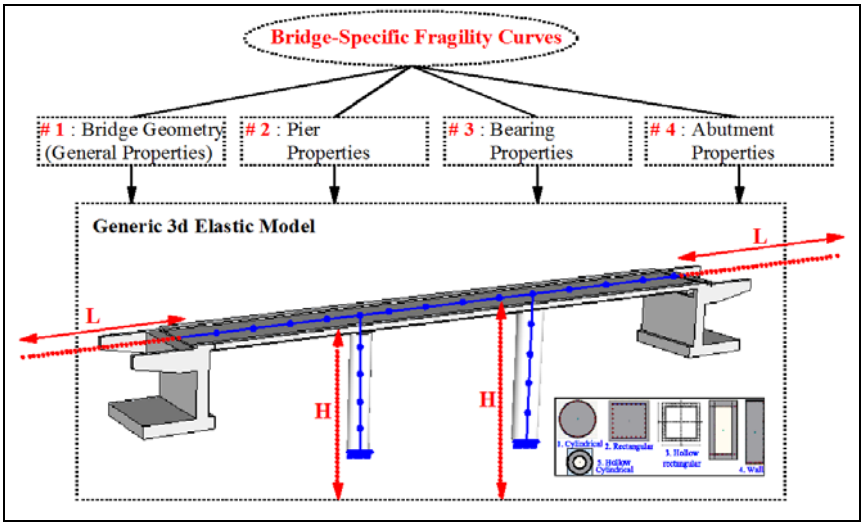

Figure 2: Input data for the derivation of bridge-specific fragility curves

(linear springs for bearings and abutments) in order to estimate seismic demand on each component. Seismic analysis is performed at bridge level, in order to consider the correlation of different components during the evaluation of bridge seismic performance for different levels of earthquake intensity. However, since the main target of the methodology is the feasibility to apply to a large bridge inventory, elastic response spectrum analysis is used for the demand calculation. To account for inelastic performance of the bridge system under seismic actions, the uncertainty in demand is calculated using nonlinear response history analysis for selected accelerograms and various intensity levels (Incremental Dynamic Analysis). Representative bridges of each category (according to the classification scheme described in §2) are selected and Monte Carlo simulation with Latin Hypercube sampling is performed in order to quantify the uncertainty in seismic demand; in a practical context, uncertainty in demand is assumed to be the same for bridges classified in the same category. Having defined capacity and demand at a component level, bridge fragility is calculated assuming (conservatively) series connection between components (except for limit state 4, see §4). Since the demand calculation is based on the results for an elastic model (linear springs), the effect of gap closure should be accounted for, considering two models (open and closed gap), retaining the results of the first model until gap closure. The methodology outlined above, is described in detail in the following paragraphs.

3.1 Step 1 : Component Threshold Limit State values (Capacity) and correlated uncertainty

During the first step, threshold limit state (capacity) values are defined in terms of global engineering demand parameters. Displacement of the component control point is used, since it can be easily recorded during analysis and is a representative measure of the system's seismic performance (damage); therefore it should be correlated to local (component) damage. As far as bridge piers are concerned, the main objective is to develop a database including all different pier types shown in Table 1. Damage is initially quantified at section level (figure 3), using local engineering demand parameters (curvature) corresponding to material strain limits and developed crack widths. Moment - curvature analyses for varying geometric, material,

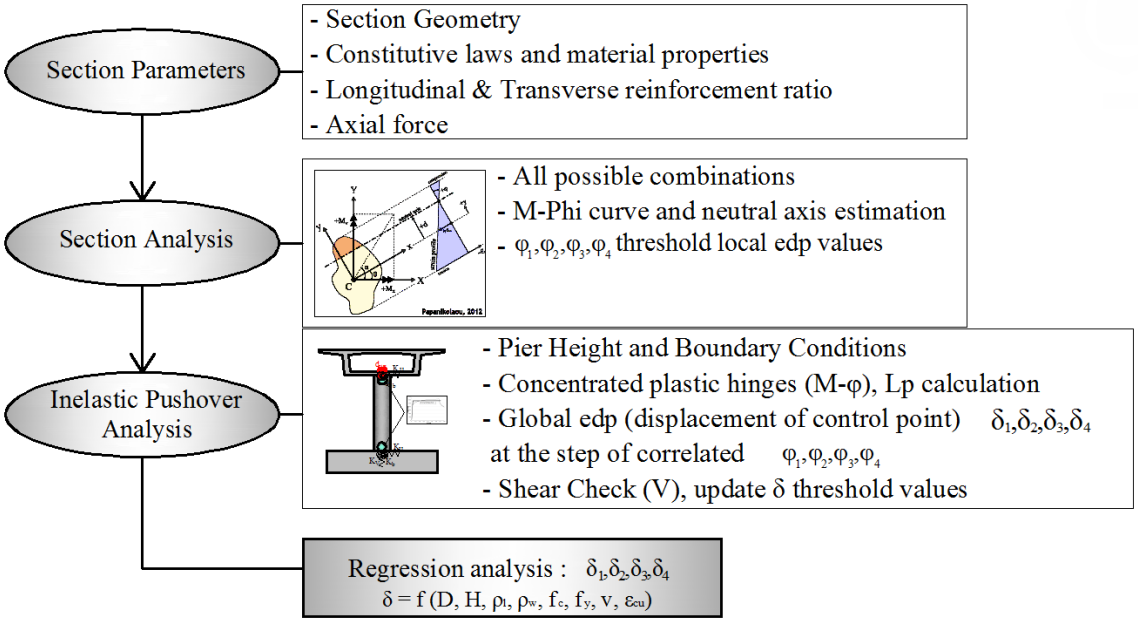

Figure 3: Component (piers) threshold limit state values in displacement terms

reinforcement and loading properties are performed, defining threshold limit state values in curvature terms and the secant stiffness of the fully cracked section at yield ($EI_{eff}=M_y/\varphi_y$), to be used as input in component analysis. Varying pier heights are considered for each different pier type and inelastic pushover analyses of piers are performed. Displacement values at pier top (component control point) for the time step that section curvature exceeds the threshold limit state value are recorded in order to define threshold limit state values in displacement terms. Shear failure modes are also considered, therefore shear checks of the pier model are performed, comparing the shear force to shear capacity ($V_u = V_c(\mu_\varphi)+V_w+V_p$). Displacement value at the time step that the developed shear force exceeds the relevant capacity is recorded and the relevant threshold displacement value is corrected, i.e. the minimum of the top displacements corresponding to flexural and shear failure modes is considered. Regression analysis for every different pier type is performed and empirical closed-form relationships are proposed for each case (pier type). The proposed empirical relationships can be used when the relevant properties are known, however it should be noted at this point that threshold values in displacement terms (capacity) are strongly dependent on the boundary conditions, namely the pier to deck connection and the foundation support. Since, as depicted in figure 3, the control point displacement (cantilever top) can be correlated to the top/bottom moment ratio (point of contraflexure), modal analysis for the first translational mode of the 3d generic beam model of the bridge studied should be initially performed to define the height x_o of the contraflexure point and subsequently calculate threshold limit state values using the proposed closed-form relationships and considering the effect of the component boundary conditions.

Uncertainty in the threshold limit state value definition in displacement terms (d_1,d_2,d_3,d_4) is calculated for each pier type separetely. Uncertainty in material properties, namely the concrete compressive strength (f_c) and steel yield strength (f_y), the ultimate concrete stain (e_{cu}) and the plastic hinge length (L_{pl}) is considered and Monte Carlo simulation with Latin Hypercube sampling is carried out for N=100 statistically different, yet nominally identical, realizations. Analyses results are processed and logarithmic standard deviations β_c are derived for every different pier type. Finally, uncertainty in the limit state definition (β_{LS}) is calculated based on statistical analysis of data (threshold values) available in the literature.

Threshold limit state values are defined in displacement terms for bridge bearings and abutments, based on the literature [10], [11], considering different failure modes, namely yielding of steel shims, lift-off, rotation and unseating for elastomeric bearings, and backwall damage, as well as abutment soil yielding and deformation for seat-type abutments. Damage states for pot bearings are additionally defined based on experimental data [12]. Uncertainty in limit state definition is calculated for abutments and bearings as well (β_{LS}).

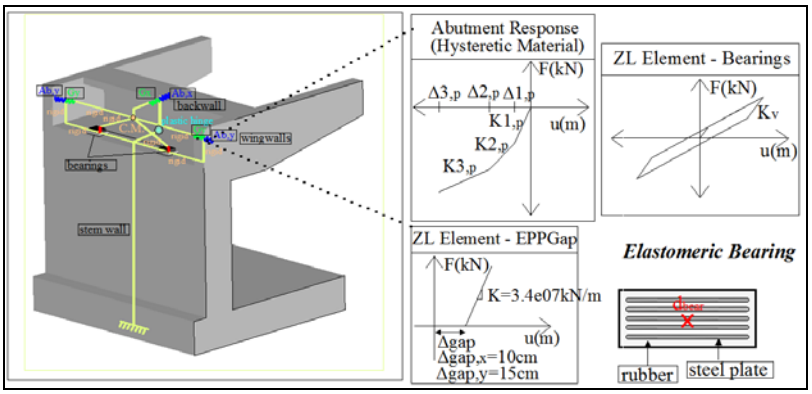

Figure 4: Component (abutments &piers) threshold limit state values in displacement terms

3.2 Step 2 : Component Demand and Bridge System Fragility

So long as threshold limit state values (capacity) and the associated uncertainty are defined, the demand at the control point of every component should be estimated in order to derive fragility curves for each limit state. The proposed methodology is based on elastic response spectrum analysis, and the equal displacement approximation ($d_{elastic}=d_{inelastic}$) for the seismic demand estimation, a reasonable assumption for T>0.5~0.6sec, which is the case for most bridges. A simplified elastic model, as depicted in figure 2 (linear springs for bearings and abutments) has to be set up, to which member properties are fed. The pier cracked stiffness ($EI_{eff}=M_y/\varphi_y$) is calculated for all piers based on empirical relationships proposed for yield moment and curvature (e.g. $\varphi_y=f\,[(f_c/f_y,v,\rho_l,\rho_w)/D]$ for cylindrical sections/bilinear M-φ section diagram). It should be noted that in the longitudinal direction of the bridge, analysis of a single-degree-of-freedom system is generally sufficient; however this is not the case for the transverse direction, since the displacement profile is strongly dependent on the deck geometry and the boundary conditions at the abutments.

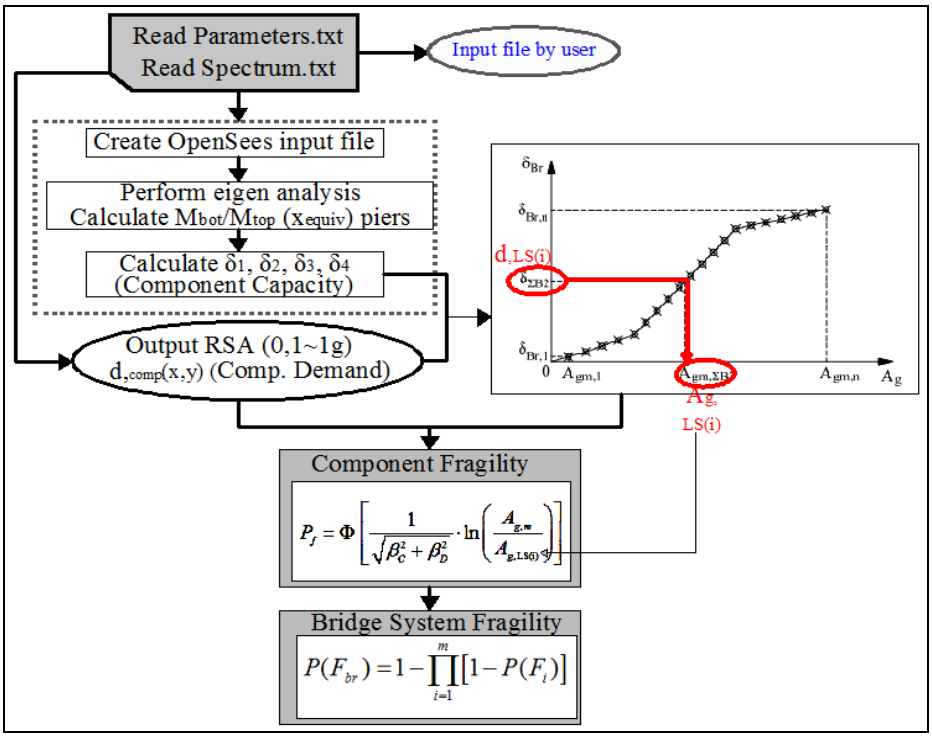

Figure 5: Outline of the proposed methodology for the derivation of bridge-specific fragility curves

Response spectrum analysis (for a site-specific spectrum or mean spectrum of selected accelerograms scaled from 0.1g to 1.0g) is performed and the displacement demand at the component control point versus earthquake parameter is plotted, representing the evolution of damage parameter (displacement) with increasing earthquake intensity (PGA=0.1g~1.0g in this case). From this diagram, median threshold values of the earthquake intensity parameter can be obtained for every damage state (figure 5). Apart from mean values, the standard deviation corresponding to the total demand and capacity uncertainty value, under the assumption of statistical independence, should be defined. Since uncertainty in capacity is calculated in step 1, uncertainty in demand is defined at this step, based on the results of detailed structural models and nonlinear analysis of representative bridge types (according to the classification scheme described above). Uncertainty in material properties, gap size, bearing stiffness and soil properties are considered during analysis of representative bridges; as noted previously,

reduced Monte Carlo simulation for N=100 samples is used and Incremental Dynamic Analysis for selected accelerograms scaled to different levels of earthquake intensity is performed in order to calculate β_d for the relevant bridge class.

Bridge-specific fragility curves are calculated on the basis of the above (mean and standard deviation values), assuming series connection between components, except for LS4 corresponding to bridge collapse and related to collapse of bridge piers only. As already outlined, fragility analysis is based on the response spectrum results of two simplified models (open and closed gap), retaining results of the first model until gap closure.

Application of the methodology presented herein is presented in the following paragraphs, providing the empirical closed-form relationships for the quantitative definition of threshold limit state values (capacity) of all different bridge pier types, the relevant β_c and β_{LS} values, as well as the β_d values for 3 different bridge classes (#221, #232, #221).

4 BRIDGE COMPONENT CAPACITY AND ASSOCIATED UNCERTAINTIES

Different geometric, reinforcement, material and loading parameters affect the available strength and ductility, and eventually the seismic performance of piers. The fact that a cylindrical pier designed according to the provisions of EC2 and EC8 will eventually have a different threshold limit state value (considered limit states are 1 to 4, see Table 2) compared to a similar pier not being designed according to code provisions (reinforcement ratio, confinement) or a pier with different axial load and even more, compared to a hollow rectangular or a wall pier, is recognised. The effect of different pier types, dimensions, material properties and constitutive laws, longitudinal and transverse reinforcement ratio and finally axial load on the threshold limit state values was evaluated and closed form relationships are proposed here for different pier types.

Limit State (LS)	Threshold values of curvature (φ)	Quantitative Performance Description
LS 1 – Minor/Slight damage	$\boldsymbol{\varphi_1}$:φ_y	Quasi-elastic behaviour – Cracks barely visible.
LS 2 – Moderate damage	$\boldsymbol{\varphi_2}$: min (φ: $\varepsilon_c > 0.004$, φ: $\varepsilon_s \geq 0.015$)	Spalling of the cover concrete, strength may continue to increase – Crack width 1-2mm.
LS 3 – Major/Extensive damage	$\boldsymbol{\varphi_3}$: min (φ: $\varepsilon_c \leq 0.004 + 1.4 \cdot \rho_w \cdot \frac{f_{yw}}{f_{cc}}$, φ: $\varepsilon_s \geq 0.06$)	First hoop fracture, buckling of longitudinal reinforcement, initiation of crushing of concrete core – Crack width>2mm.
LS 4 – Failure/Collapse	$\boldsymbol{\varphi_4}$: min (φ: $M < 0.85 \cdot M_{\max}$, φ: $\varepsilon_s \geq 0.075$)	Loss of load-carrying capacity - Collapse

Table 2: Component Piers: Threshold limit state values (local edp)

In line with the above, different properties for all the aforementioned parameters are selected and moment-curvature analysis of all possible combinations is performed as described in figure 6. It should be noted that the parameters considered fall, in most cases, within the prescribed code requirements, however lower strength classes for concrete and steel are additionally considered, in order to include cases of older bridge piers. In-house developed software [13] that incorporates stress-strain models for confined, unconfined concrete [14], [15] and steel is used for moment-curvature analysis. Threshold values for the different limit states are initially defined in curvature terms (local engineering demand parameter) as depicted in

table 2. Empirical relationships for the estimation of secant stiffness of the fully cracked section at yield ($EI_{eff}=M_y/\varphi_y$) are proposed for every different pier type (equation 1, figure 7 – cylindrical piers).

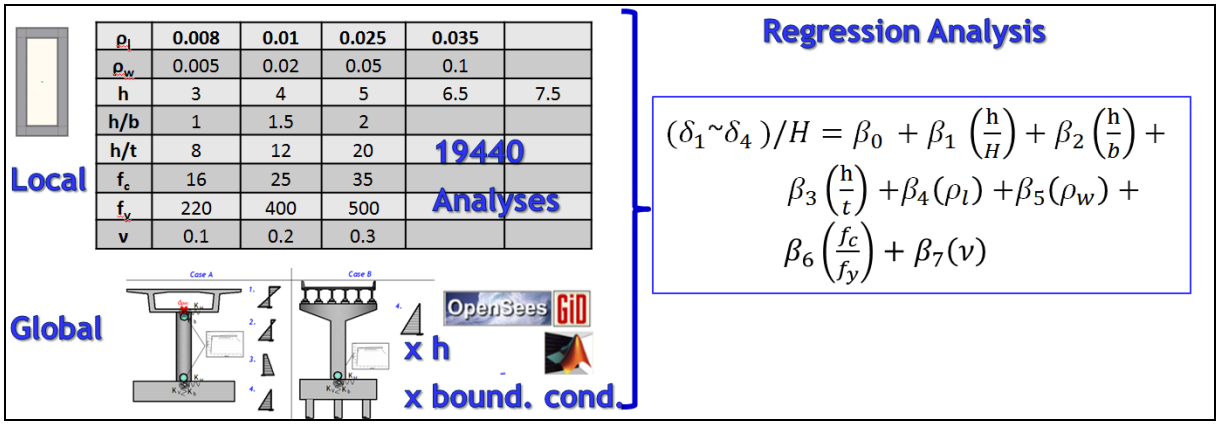

Figure 6: Bridge piers: Local to global engineering demand parameter mapping

$$\varphi_y = \exp[-5.76 - 0.736 \cdot \ln(f_c / f_y) - 0.01 \cdot \ln(v) + 0.295 \cdot \ln \rho_l + 0.091 \cdot \ln \rho_w] \cdot D$$
$$M_y = \exp[-0.339 - 0.638 \cdot \ln(f_c / f_y) + 0.224 \cdot \ln(v) + 0.5578 \cdot \ln \rho_l + 0.0557 \cdot \ln \rho_w] \cdot (2 \cdot \pi \cdot R^3 \cdot f_{cd}) \quad (1)$$

Since the main goal is to define bridge capacity and threshold limit state values in displacement terms, an inelastic generalised single-degree of freedom model is set up. All different bridge pier section types are analysed, namely cylindrical, hollow cylindrical, rectangular, hollow rectangular and wall type, while different pier height range is considered according to the pier type (i.e. 5~20m for cylindrical pier type and 20~50m for hollow rectangular). It should be noted that both weak and strong axis orientation were examined for rectangular shaped piers. Lumped plasticity model is used (bilinear moment-curvature curve), while the plastic hinge length is taken equal to $L_{pl}=0.09L_s+0.2h$ for rectangular, hollow rectangular and wall type piers and $L_{pl}=0.09L_s+2D/3$ for circular and hollow circular according to [16] .

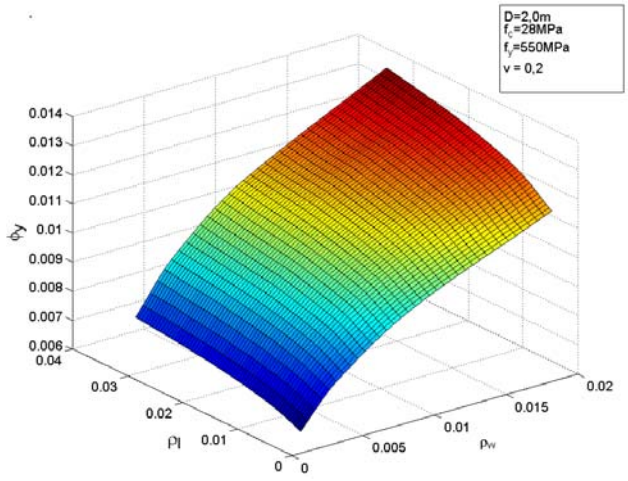

Figure 7: φ_y-ρ_l-ρ_w diagram for cylindrical piers

Nonlinear static (pushover) analyses of the single-degree of freedom models are performed individually for each pier type case (and both strong and weak axis orientation) and the displacement of cantilever top (component control point) at the time step that the deformation of

the plastic hinge exceeds threshold limit state values ($\varphi_1,\varphi_2,\varphi_3,\varphi_4$ in table 2) is recorded. Shear failure mode is considered, since the shear demand at each step is compared with the ultimate shear capacity and the displacement value associated with LS4 is recorded and compared with the one derived considering flexural failure. It should be recalled at this point that the reduction in the V_c contribution with increasing curvature ductility is considered.

Practically all possible combinations of properties and pier heights are considered (e.g. ~51800 analyses for the case of hollow rectangular piers) and threshold limit state values in displacement terms ($\delta_1,\delta_2,\delta_3,\delta_4$) are obtained. Analysis results are processed using the advanced least squares method (robust fit) and empirical relationships for threshold δ_i values are provided for every different pier type (equations 2 for the case of cylindrical piers).

Depending on the boundary conditions, i.e. the type of pier to deck connection and the type of foundation, the moment pier diagram may vary, as shown in figure 8. Therefore the equivalent cantilever height x_o, corresponding to the height of the contraflexure point should be estimated in order to use the proposed empirical relationships, derived from cantilever analysis.

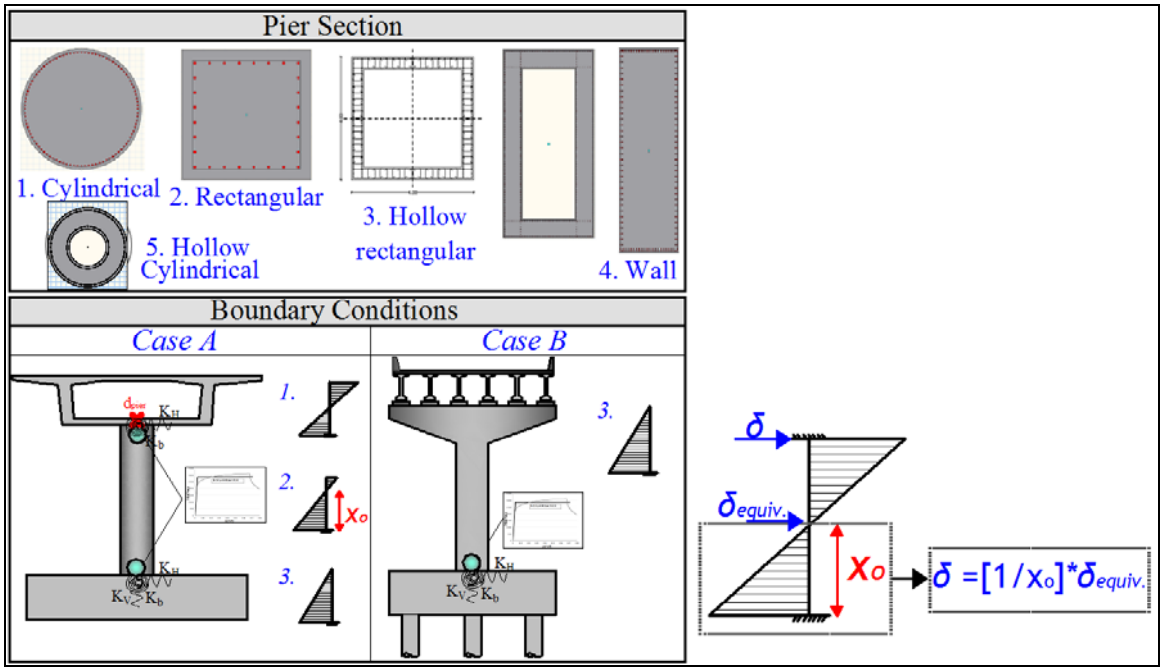

Figure 8: Pier types and boundary conditions

$$\begin{aligned}
\delta_1 &= \exp[-6.600-0.892\cdot\ln(D/H)-0.003\cdot\ln(\nu)-0.700\cdot\ln(f_c/f_y)+0.089\cdot\ln(\rho_w)+0.275\cdot\ln(\rho_l)]\cdot H\\
\delta_2 &= \exp[-5.594-0.553\cdot\ln(D/H)-0.288\cdot\ln(\nu)+0.027\cdot\ln(f_c/f_y)+0.026\cdot\ln(\rho_w)-0.110\cdot\ln(\rho_l)]\cdot H\\
\delta_3 &= \exp[-2.909-0.415\cdot\ln(D/H)-0.243\cdot\ln(\nu)-0.403\cdot\ln(f_c/f_y)+0.505\cdot\ln(\rho_w)-0.122\cdot\ln(\rho_l)]\cdot H\\
\delta_4 &= \exp[-2.560-0.369\cdot\ln(D/H)-0.339\cdot\ln(\nu)-0.398\cdot\ln(f_c/f_y)+0.384\cdot\ln(\rho_w)+0.019\cdot\ln(\rho_l)]\cdot H
\end{aligned} \quad (2)$$

The empirical relationships proposed are applied and results regarding all different pier types examined are presented in figures 9 and 10 in terms of dimensionless parameters (displacement ductility and drift) for them to be comparable. Curvature at yield and available curvature ductility (related to displacement ductility via the plastic hinge length) of hollow rectangular and wall pier type sections is less compared to circular, hollow circular and rectangular section. However, the fact that different constitutive models for confined concrete are used for the case of circular [14] and rectangular sections [15] should be highlighted, since the results are dependent on the ultimate strain value ε_{cu}.

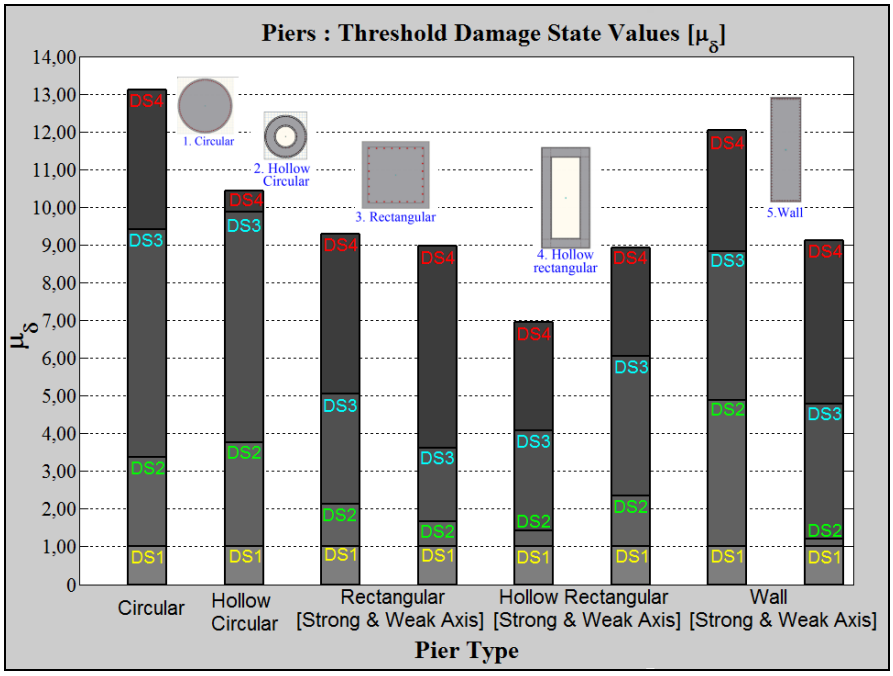

Figure 9: Displacement ductility for all limit states and pier types

As depicted, the threshold capacity values for the four limit states considered (minor, major, extensive and collapse), vary depending on the pier type, therefore a uniform value may either overestimate or underestimate the component's capacity. Detailed results regarding pier component capacity can be found in the technical report of RETIS-Risk (Aristeia II) research programme (expected to be available in July 2015).

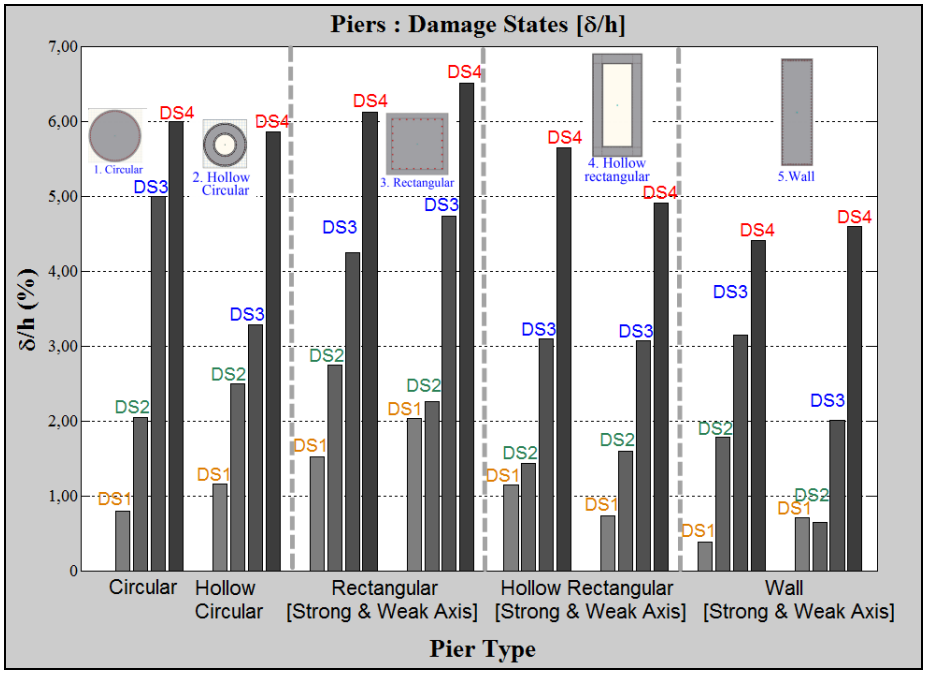

Figure 10: Drift for all limit states and pier types

Uncertainty in capacity is considered, assuming the distribution of random variables with mean and standard deviation values as shown in Table 3, according to [11], [17]. Again, Latin Hypercube sampling is used for 100 realizations of each different pier type. Analysis results

are processed and β_c values are proposed for every different pier type and limit state. For example, analysis of the sample size of cylindrical bridge piers resulted in different β_c values for every limit state, in particular β_{c1}=0.22, β_{c2}=0.35, β_{c3}=0.44, β_{c4}=0.53.

Random Variable	Distribution	Mean	COV
f_c (MPa)	normal	34.5	18%
f_y (MPa)	normal	463	8%
$\varepsilon_{cu}/\varepsilon_{cu,conf.\ model}$ (%)	normal	0.99	35.8%
L_{pl} / $L_{pl(Biskinis)}$	uniform	0.96	47.4%

Table 3: Assumed distributions for random variables related to pier capacity)

Limit state definitions for the abutments are given in Table 4 [11]. Inelastic static (pushover) analysis is performed for the abutment subsystem in order to define the threshold value in terms of displacement of the control point for the first limit state (the other three states are directly expressed in terms of fractions of the backwall height).

Limit State	Threshold values	Quantitative Performance Description
LS 1 – Minor/Slight damage	$\mu_{\varphi,backwall}$=1.5	Cracking and significant damage to the backwall
LS 2 – Moderate damage	$d = 0.01 \cdot h_{backwall}$	First yield of the abutment soil
LS 3 – Major/Extensive damage	$d = 0.035 \cdot h_{backwall}$	Excessive deformation of abutment soil
LS 4 – Failure/Collapse	$d = 0.1 \cdot h_{backwall}$	Ultimate deformation of abutment soil (cohessionless soil)

Table 4: Component Abutments: Threshold limit state values (global edp)

Limit State	Threshold values of shear strain (γ)	Quantitative Performance Description
LS 1 – Minor/Slight damage	100%	Initiation of nonlinear behaviour, potential yielding of anchor bolts and cracking of pedestals.
LS 2 – Moderate damage	150%	Visible damage to the bearing. Yield of steel shims.
LS 3 – Major/Extensive damage	200%	Lift off at the edge of the bearing, uplift and rocking. May cause delamination, bonding failure between rubber layers and steel shim plates.
LS 4 – Failure/Collapse	250%	Lift-off, rotation. Unseating, failure of bearings.

Table 5: Component Bearings: Threshold limit state values (global edp)

The engineering demand parameter used to define threshold limit state values for elastomeric bearings is the shear strain (γ=d/$t_{,rubber}$); threshold values based on information from the literature are given in Table 3. Pot bearings, frequently used in modern motorway bridges, have different failure modes and therefore threshold limit state values. Minor damage is related to the displacement that the lateral load exceeds 10% of the vertical load [12], while moderate, major and collapse limit states are defined according to [12].

5 BRIDGE COMPONENT SEISMIC DEMAND AND ASSOCIATED UNCERTAINTIES

As already mentioned, the median threshold value of the earthquake parameter (PGA,S_a,S_d) for every damage state is calculated using response spectrum analysis results for scaled accelerograms, based on the equal displacement approximation ($d_{elastic}$=$d_{inelastic}$). The main objective of the proposed methodology is the derivation of fragility curves for the longitudinal and transverse direction of the bridge, representing the conditional probability of reaching or exceeding a limit state as a function of the selected ground motion intensity parameter. Fitting of fragility analysis results to a lognormal distribution to express results in a probabilistic manner, requires the mean and standard deviation value for each component.

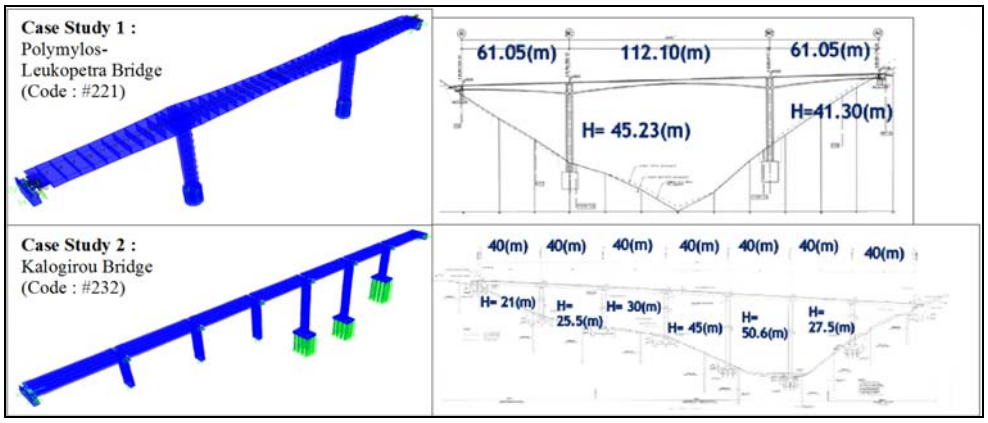

Figure 11: Case Study Bridges

Random Variable	Distribution	Mean	COV
f_c	normal	34.5 MPa	18%
f_y	normal	506 MPa	8%
gap size	normal	24.5 cm	20%
bearings	uniform	G=0.9 MPa	22%
soil properties	uniform	G=663 MPa	20%

Table 6: Assumed distributions for random variables (uncertainty in demand)

A Probabilistic Seismic Demand Model (PSDM) is used to estimate the dispersion value, representing the uncertainty in demand. It is recalled that there are two approaches regarding the implementation of the PSDM, namely the "cloud" (Probabilistic Seismic Demand Analysis) and the "scaling" (Incremental Dynamic Analysis) approach, with the latter having the advantage of not requiring an a priori assumption for the probabilistic distribution of seismic demands for fitting fragility curves [7]. The approach implemented herein is IDA for different levels of seismic action ranging from 0.1~1g. The limit state probability of exceedance at a specific IM level equals the occurrence ratio of the specific limit state, defined as the ratio of the number of damage cases n_i, for the damage state i over the number of simulations N, i.e.

$$P[(\mathrm{D} \geq \mathrm{DS}_i \,|\, I_M) = \frac{n_i}{N} \quad (\mathrm{i} = 1 to 4) \tag{3}$$

$$P[(\mathrm{D} \geq \mathrm{LS} | I_M) = \int_{-\infty}^{I_M} \frac{1}{I_M \cdot \sqrt{2\pi \cdot \hat{\beta}}} \cdot e^{\left\{ -\frac{[\ln(I_M) - \hat{\mu}]}{2 \cdot \hat{\beta}^2} \right\}} d(\mathrm{I}_M) \quad (4)$$

Standard deviation, is calculated for every bridge component (piers, bearings, abutments) based on the results of nonlinear response-history analysis of all the realizations considered and different levels of A_g. Their values are obtained from equation 5, where *M* is the number of realizations and a_i is associated with the onset of collapse for the i^{th} realization [18].

$$\hat{\beta} = \sqrt{\frac{1}{(\mathrm{M}-1)} \cdot \sum_{i=1}^{\mathrm{M}} (\ln(\mathrm{a}_i) - \hat{\mu})^2} \quad (5)$$

Two representative bridges of the most common categories in Greek motorways (#221-Polymylos-Leukopetra bridge and #232-Kalogirou bridge according to the classification scheme presented in §2) are studied. Another common category (overpass #121) has been studied and results can be found elsewhere [19], however they are briefly presented herein as well. Both case study bridges are part of the Egnatia Motorway. The structures are modelled and analysed using the OpenSees platform. For the formulation of the 3d model, elastic beam-column elements are used for the deck and beam-column with hinges (lumped plasticity) elements for the piers, as depicted in figures 12 and 13. Cross section analysis was performed for the piers to obtain moment-curvature diagrams for the potential plastic hinges (pier top and bottom for the case of monolithic pier-to-deck connection and pier bottom only for the case of connection through bearings), while the plastic hinge length L_p was calculated according to [16]. The abutment-backfill interaction (passive earth pressures) after gap closure was considered according to [11] .

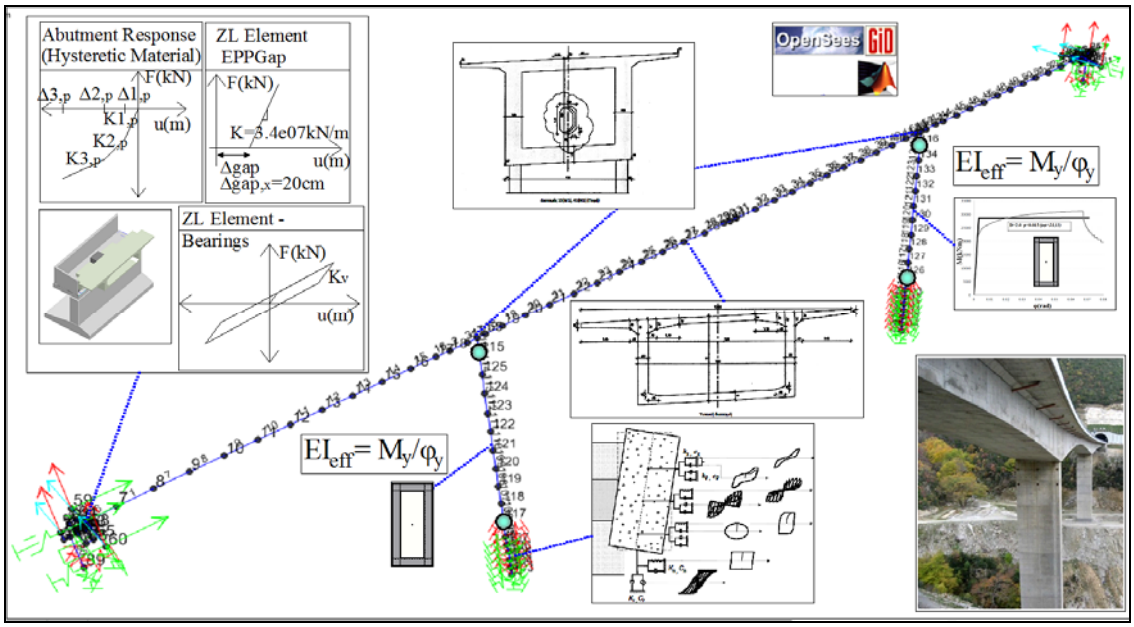

Figure 12: Polymylos-Lefkopetra Bridge (#221)

Uncertainty in demand is considered, assuming the distribution of random variables with mean and standard deviation values as shown in Table 6 [17], [20], [21]. Again Latin Hypercube sampling is used for 100 realizations of each different bridge. Accelerograms (7) for re-

sponse history analysis were selected using ISSARS (M=6.6~6.8 and R=20~40) and scaled according to EC8-Part 2 provisions [22]. A Matlab-code was generated in order to perform analysis for all realizations and various levels of earthquake intensity (i.e. 0.1~1g) resulting in a total of 7×10×100=7000 analyses for every bridge and every direction, and standard deviation value was calculated for all components considered.

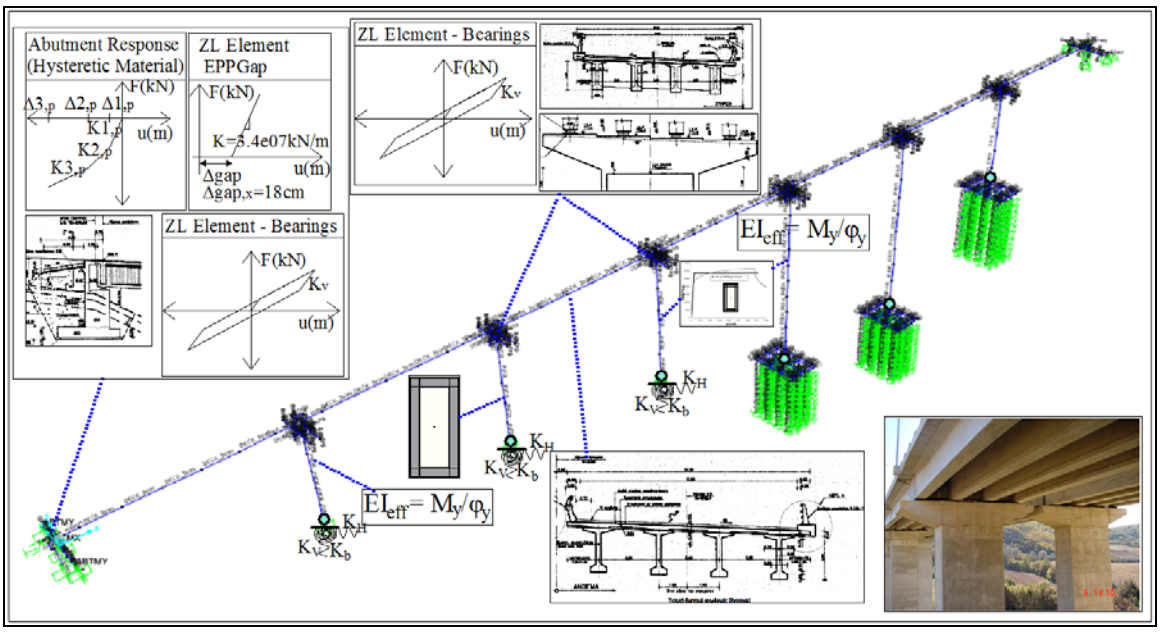

Figure 13: Kalogirou Bridge (#232)

Both cases studies involve long bridges, constructed in the early 2000s, having tall hollow rectangular piers monolithically connected to the deck in the case of Polymylos-Leukopetra bridge and connected through bearings in the case of Kalogirou bridge. Bridge piers are designed according to current provisions. Dispersion values for piers and bearings of the bridges studied are presented in tables 7 and 8. Uncertainties regarding the abutment response have not been taken into account at this stage of development (only uncertainty in gap size is included); therefore the relevant dispersion value is not presented herein.

	Polymylos_X (#221)				Kalogirou_X (#232)			
Component	$\beta_{d,LS1}$	$\beta_{d,LS2}$	$\beta_{d,LS3}$	$\beta_{d,LS4}$	$\beta_{d,LS1}$	$\beta_{d,LS2}$	$\beta_{d,LS3}$	$\beta_{d,LS4}$
Piers	26%	24%	13%	8%	30%	21%	15%	10%
Bearings	20%	18%	12%	10%	26%	19%	15%	11%

Table 7: Uncertainty in demand - β_d values for Polymylos and Kalogirou Bridge (X direction)

	T7_X OverPass (#121)			
Component	$\beta_{d,LS1}$	$\beta_{d,LS2}$	$\beta_{d,LS3}$	$\beta_{d,LS4}$
Piers	36%	30%	18%	12%
Bearings	29%	28%	22%	20%

Table 8: Uncertainty in demand - β_d values for T7 Overpass (X direction)

6 BRIDGE SYSTEM FRAGILITY

Bridge component capacity and demand as well as related uncertainties are calculated utilising the proposed methodology. The total uncertainty value is calculated for every component according to equation 6, under the assumption of statistical independence.

$$\beta_{tot} = \sqrt{\beta_C^2 + \beta_D^2 + \beta_{LS}^2} \tag{6}$$

Series connection between components is assumed for the calculation of bridge fragility, according to equation 7 (i: bridge components considered; namely bridge piers, bearings, abutments).

$$P(F_{br}) = 1 - \prod_{i=1}^{m} [1 - P(F_i)] \tag{7}$$

Since collapse of the bridge system is not expected to occur if bearings or abutments reach LS4 as described previously at a component level, limit state 4 at bridge (as a system) level is related to pier collapse only. Therefore series connection assumption is not invoked for the estimation of system fragility for the collapse limit state.

Fragility analysis is based on the results of response spectrum analysis of the simplified 3d bridge model described above. Two alternative connections of bearing and abutment linear springs depicted in figure 14 are considered for seat type abutments for the case of open and closed gap, respectively. Bridge-specific fragility curves are derived using the first model analysis results up to gap closure.

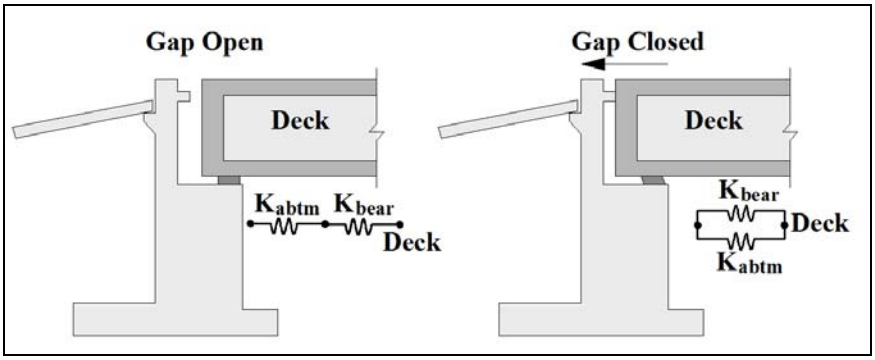

Figure 14: Pier types and boundary conditions

7 SOFTWARE DEVELOPMENT

A Matlab-based software was developed for the implementation of the previously described methodology and the derivation of bridge-specific fragility curves, briefly described in figure 15. The software is based on a generic simplified 3d bridge model created using the OpenSees platform [23]. Input data provided by the user are depicted in figure 15 and concern general bridge geometry and loading properties, component (pier, bearing, abutment) properties, and the (site-specific) response spectrum. Threshold limit state values for piers are automatically calculated according to the geometric, material, reinforcement, loading properties and boundary conditions of each case, while dispersion values, calculated in line with the previously described procedure, are included. Different boundary conditions at abutments are considered for the case of open and closed gap, and fragility curves are automatically calculated for longitudinal and transverse directions separately. The software developed is applied to 76 bridges of a Egnatia Motorway (Western Macedonia section), for the seismic assessment of the road network in the frame of RETIS-Risk (Aristeia II) research programme and

will be included in a GIS-based freeware for the management of seismic risk of roadway networks.

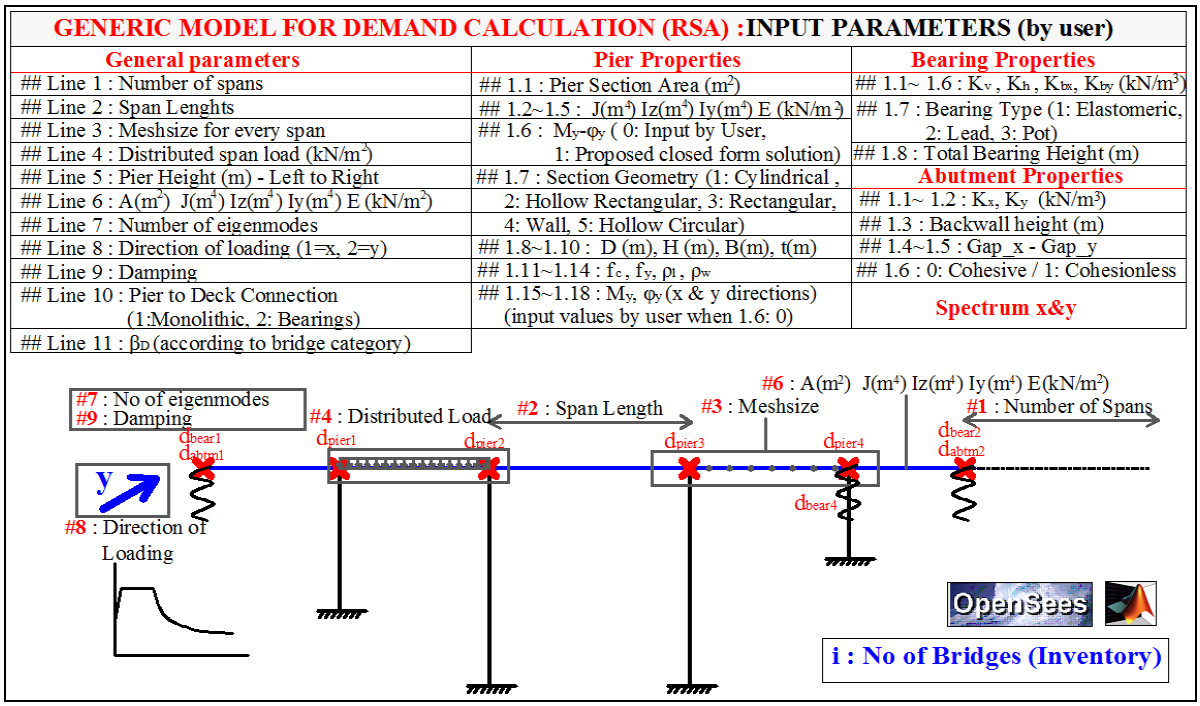

Figure 15: Input data 3d generic beam model

8 EXAMPLES OF BRIDGE-SPECIFIC FRAGILITY CURVES

Fragility curves of the two case study bridges described above are presented in Figures 16 and 17. Since bridges are designed according to code provisions, the probability that demand exceeds bridge capacity is low even for higher levels of earthquake intensity. For both bridges, the lower limit states are controlled by bearing damage, since the yielding of piers occurs for higher levels of earthquake intensity. Regarding the collapse limit state for the system, it is controlled by pier collapse limit state only, as discussed in section 6.

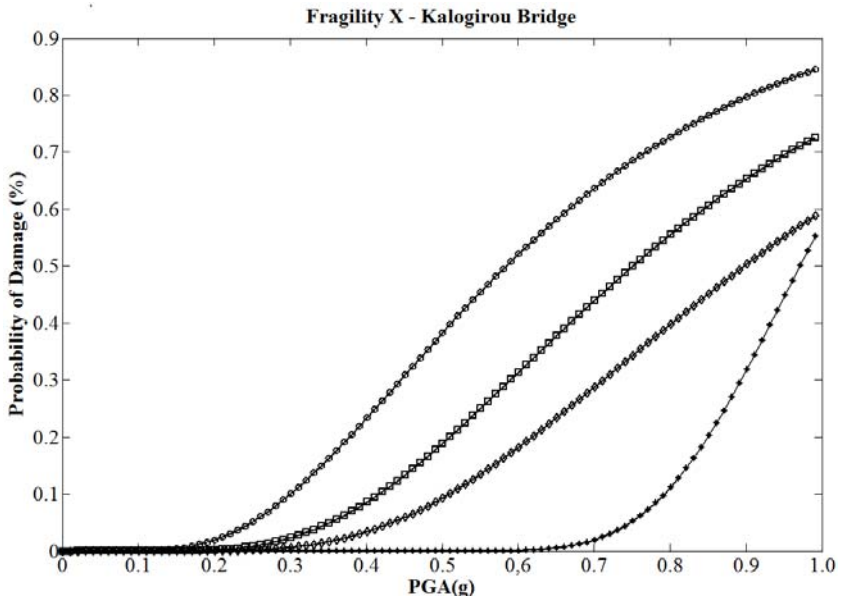

Figure 16: Fragility longitudinal direction (Kalogirou bridge)

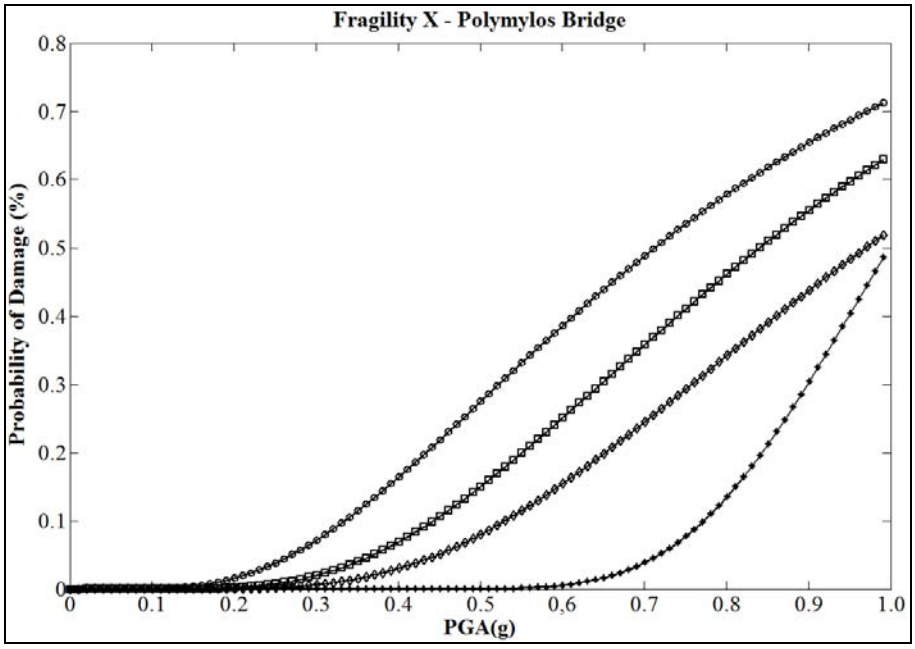

Figure 17: Fragility longitudinal direction (Polymylos Bridge)

It has to be noted that, as evident from Figures 16 and 17, the uncertainty (β_{tot}) associated with each individual fragility curve is generally different (see also Tables 7, 8), hence the different shape of the curves and the possibility of intersecting curves (e.g. for Polymylos Bridge when PGA exceeds about 1.0g). This is still a controversial issue worldwide, since while it is widely recognised that the uncertainty is different for each type, intersection of fragility curves is conceptually incorrect.

9 CONCLUSIONS

The conclusions reached at this stage of this ongoing study can be summarised as follows:

- All critical components should be considered for the derivation of bridge fragility curves. In addition to those addressed herein (piers, abutments, bearings), one could also consider foundation elements that might be critical in some bridge types.
- Threshold limit state values of components should be expressed in global terms (typically displacements) and correlated to relative local damage.
- Different geometry, material, reinforcement, loading properties as well as boundary conditions, affect component capacity and threshold limit state values and should be taken under consideration during fragility analysis.
- Uncertainty in capacity, demand, and limit state definition should be estimated for every component and limit state separately.
- Bridge-specific fragility curves should be based on the results of a simplified 3d model in order to account for the correlation between different components and the dependence of the displacement profile on deck geometric properties and boundary conditions.
- Feasible methodologies for the derivation of bridge-specific fragility curves are those that can be readily applied to a bridge inventory with a view to estimating earthquake losses of a roadway network.

Acknowledgement

This research has been co-financed by the European Union (European Social Fund – ESF) and Greek national funds through the Operational Program "Education and Lifelong Learning" of the National Strategic Reference Framework (NSRF) – Research Funding Program: *ARISTEIA II: Reinforcement of the interdisciplinary and/or interinstitutional research and innovation*

The authors would like to acknowledge the fruitful discussions and the coooperation of other members of the research team of the above programme, in particualrly those working on Work Packages 2 and 8.

REFERENCES

[1] I.F. Moschonas, A.J. Kappos, P. Panetsos, V. Papadopoulos, T. Makarios, P. Thanopoulos, Seismic fragility curves for greek bridges: methodology and case studies. *Bulletin of Earthquake Engineering*, 7(2), 439-468, 2008.

[2] R. DesRoches, B. Nielson, J. Pagett, Fragility Curves for Mid-America Bridges. *8th U.S. National Conference on Earthquake Engineering*. San Fransisco, California, 2006.

[3] E. Choi, R. DesRoches, B. Nielson, Seismic fragility of typical bridges in moderate seismic zones. *Engineering Structures*, 26(2), 187-199, 2004.

[4] S. Banerjee, M. Shinozuka, Nonlinear Static Procedure for Seismic Vulnerability Assessment of Bridges. *Computer-Aided Civil and Infrastructure Engineering*, *22*(4), 293–305, 2007.

[5] D. Cardone, G. Perrone, M. Dolce, Seismic risk assessment of highway bridges. *1st US-Italy Seismic Bridge Workshop*. Pavia, Italy,2007.

[6] M. Berry, M. Eberhard, *Performance Models for Flexural Damage in Reinforced Concrete Columns*. PEER Report 2003/18, University of Washington.

[7] J. Zhang, Y. Huo, Evaluating effectiveness and optimum design of isolation devices for highway bridges using the fragility function method. *Engineering Structures,* 31, 1648-1660, 2009.

[8] P. Towashiraporn, Building Seismic Fragilities using Response Surface Metamodels. *Ph.D. Thesis,* Georgia Institute of Technology, 2004.

[9] Kappos, A., Sextos, A., Stefanidou, S., Mylonakis, G., Pitsiava, M., Sergiadis, G., "Seismic Risk of Inter-Urban Transportation Networks", Procedia-Economics & Finance vol. 18, 2014, 263 – 270.

[10] A. Mori, P.J. Moss, N. Cooke, A.J. Carr, The Behavior of Bearings Used for Seismic Isolation under Shear and Axial Load. *Earthquake Spectra,* 15(2), 199-224, 1999.

[11] B.G. Nielson, Analytical Fragility Curves for Highway Bridges in Moderate Seismic Zones. *Ph.D. Thesis,* Georgia Institute of Technology, 2005.

[12] J.F. Stanton, C.W. Roeder, T.I. Campbell, *High-Load Multi-Rotational Bridge Bearings.* NCHRP Report 432, National Academy Press, Washington, 1999.

[13] V.K. Papanikolaou, Analysis of arbitrary composite sections in biaxial bending and axial load. *Computers and Structures*, 98-99, 33-54, 2012.

[14] J.B. Mander, M.J.N. Priestley, R. Park, Theoretical Stress-Strain Model for Confined Concrete. *Journal of Structural Engineering*, 114(8), 1804-1826,1988.

[15] A.J. Kappos, Analytical Prediction of the Collapse Earthquake for R/C Buildings: Suggested Methodology. *Earthquake Engineering and Structural Dynamics*, 20, 167-176, 1991.

[16] D. Biskinis, Strength and deformation capacity of as-built and retrofitted R/C members. *Ph.D. Thesis,* University of Patras, 2007. (in greek)

[17] C. Dymiotis, A.J. Kappos, M.K. Chryssanthopoulos, Seismic Reliability of R/C Frames with Uncertain Drift and Member Capacity. *Journal of Structural Engineering*, 125(9), 1038-1047 ,1999.

[18] K. Porter, R. Kennedy, R. Bachman, Creating Fragility Functions for Performance-Based Earthquake Engineering. *Earthquake Spectra*, 23(2), 471-489, 2007.

[19] S.P. Stefanidou, A.J. Kappos, Optimum Selection Of Retrofit Measures For R/C Bridges Using Fragility Curves. *4th ECCOMMAS Thematic Conference on Computational Methods in Structural Dynamics and Earthquake Engineering*. Kos Island, Greece, 12-14 June 2013.

[20] D. Tavares, J.Padgett, P. Paultre, Fragility curves of typical as-built highway bridges in eastern Canada. *Engineering Structures*, 40, 107-118, 2012.

[21] M. Fardis, V. Kolias, T. Panagiotakos, C. Katsaras, T. Psychogios, *Guide for Bridge Design with emphasis on Seismic Aspects.* Report No. SEE 2012-01, University of Patras.

[22] E.I. Katsanos, A.G. Sextos, ISSARS: An intergrated software environment for structure-specific earthquake ground motion selection. *Advances in Engineering Software*, 58, 70-85, 2013.

[23] F. McKeena, G.L. Fenves, *Open System for Earthquake Engineering Simlation*. Pacific Earthquale Engineering Research Center, Version 2.4.5, 2015.